Measurements and boson polarization studies with VBS processes in ATLAS

Francesco A. Conventi[1]
On behalf of ATLAS Collaborations

[1]Università Parthenope and INFN Napoli

WIN 2025
JUNE 9-13, **Sussex, Brighton (UK)**

Outline

- Semileptonic VBS and anomalous quartic gauge couplings at 13 TeV arXiv:2503.17461
- Evidence for longitudinally polarised bosons in the EW $W^{\pm}W^{\pm}$ production arXiv:2503.11317

Why Diboson or multibosons?

- In the Standard Model (SM), the non-Abelian structure of the electroweak sector predicts the self-interaction of vector bosons leading to vertices with **three** or **four vector bosons**.
- Vector boson scattering/fusion (**VBS**) processes probe the mechanism of electroweak symmetry breaking
- Measurements of cross-section and polarization to validate the standard model (SM) at TeV scale
- Triple/Quartic Gauge boson coupling (T/QGC) to search for anomalous couplings and probe new physics ➔ EFT interpretation

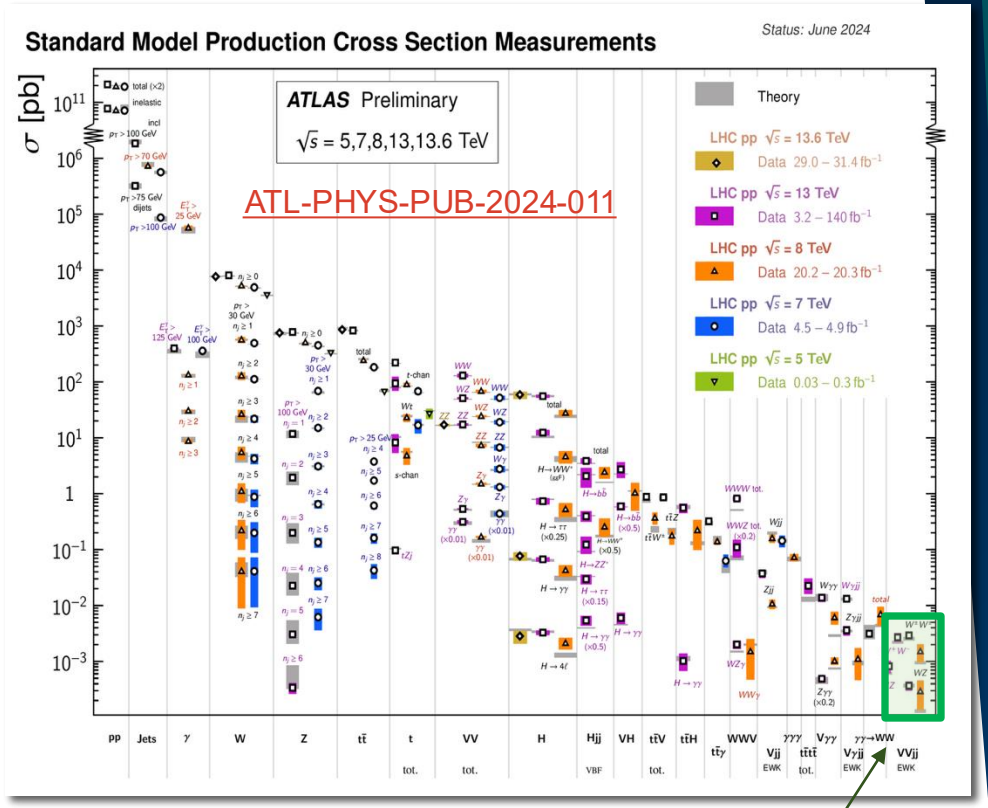

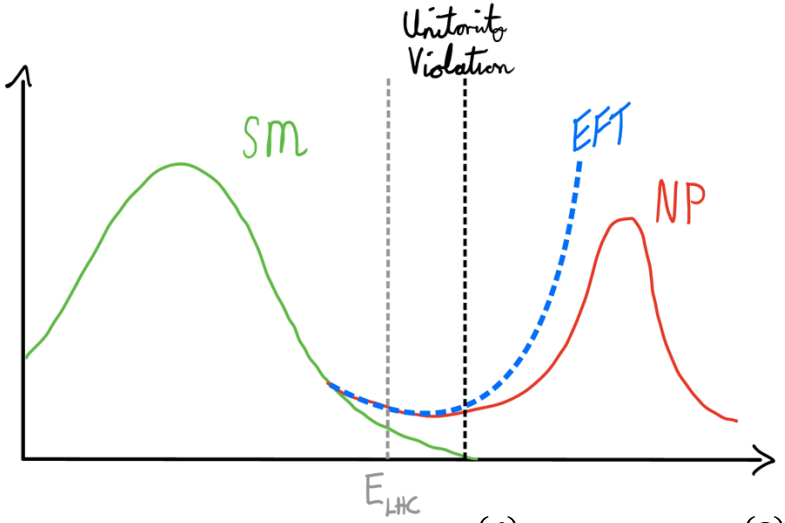

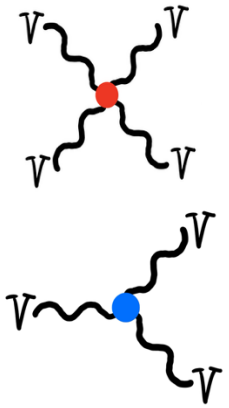

$$\mathcal{L}_{SMEFT} \approx \mathcal{L}_{SM}^{(4)} + \sum_i \frac{c_i^{(6)}}{\Lambda^2} \mathcal{O}_i^{(6)} + \sum_i \frac{c_i^{(8)}}{\Lambda^8} \mathcal{O}_i^{(8)}$$

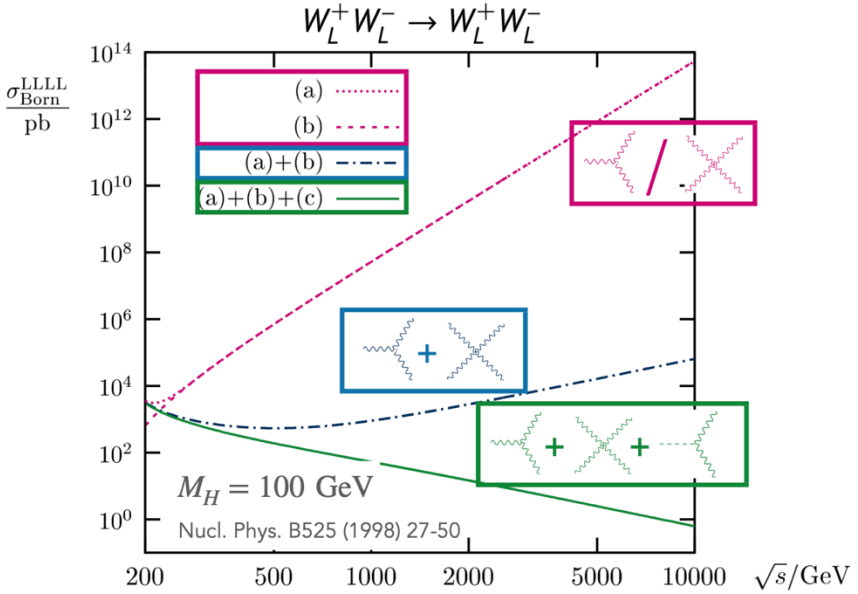

VBS Extremely Rare!

Expected fractions:

61% $W_T^{\pm} W_T^{\pm}$

29% $W_T^{\pm} W_L^{\pm}$

10% $W_L^{\pm} W_L^{\pm}$

39% $W_L^{\pm} W_L^{\pm}$

Vector Boson Scattering (VBS)

(arXiv: 2503.17461 March 2025)

Vector Boson Scattering: interaction of two vector bosons radiated from the initial-state quarks, yielding a final state with two bosons and two jets, VVjj, in a purely electroweak process

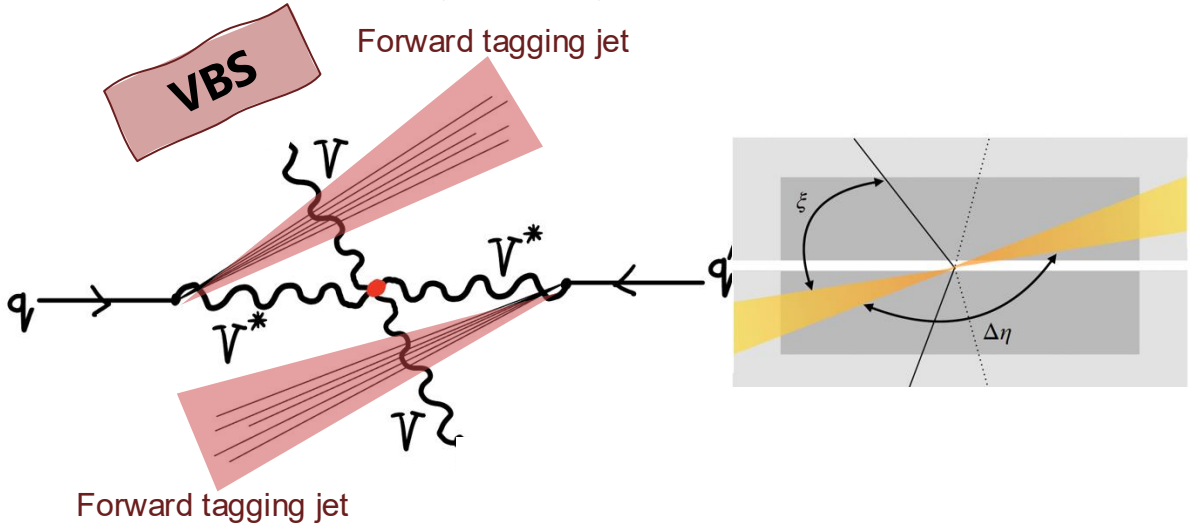

Experimentally challenging due to small xsections (~fb)

EWK production contains both VBS and non-VBS processes → cannot be dissociated

EWK VVJJ VBS

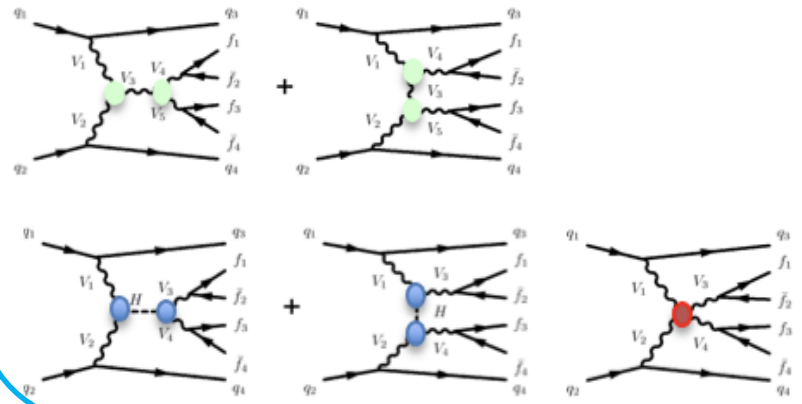

EWK VVJJ NON-VBS

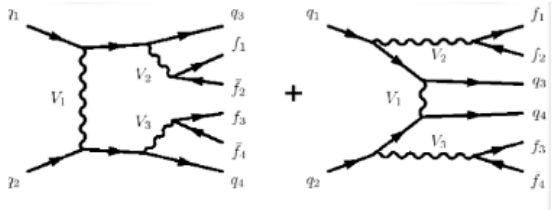

Main background: Diboson QCD production in association with two jets

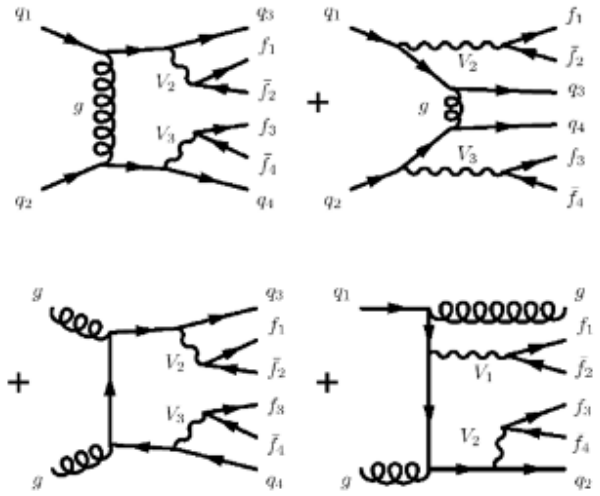

EW diboson production in semileptonic final states at 13 TeV

(arXiv: 2503.17461)

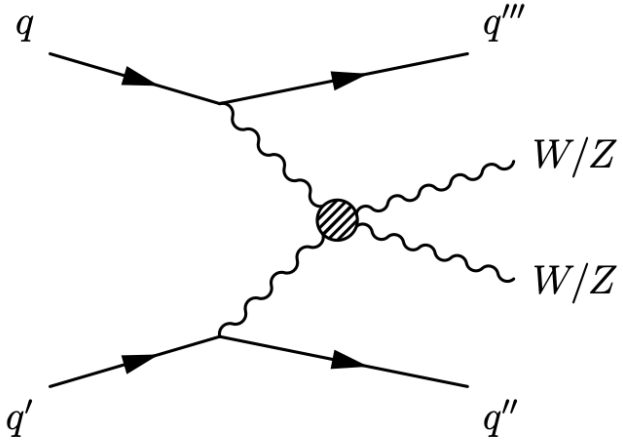

Measurement of semileptonic VBS production at 13 TeV with **140 fb^{-1}**

- After **0,1,2 leptons** categorization and **VBS topology tagging jets** require **Hadronic boson decay** (small/large-jets): Merged **or** resolved regions

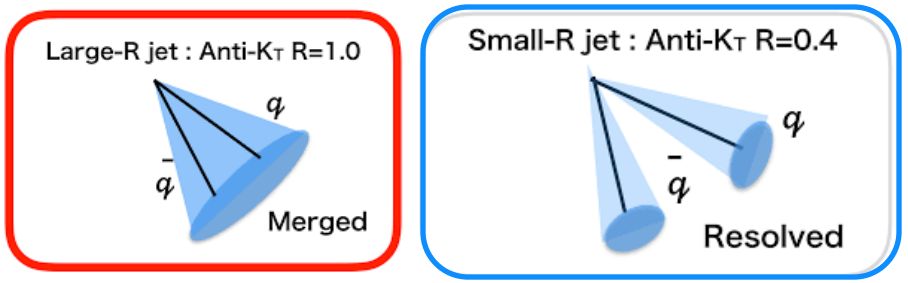

- **3 Variables Boson tagger** (mass, n_tracks, D_2) designed to provide constant efficiency independent of the jet p_T applied to large-R jets to select those consistent with V→qq 2-prong decays:
  - **Pass 80%** Efficiency boson tagger → **Merged HP**
  - **Pass 50%**, **Fail 80%** Efficiency boson tagger → **Merged LP**
  - **Fail Merged selection** → **Resolved**

Analysis Flow

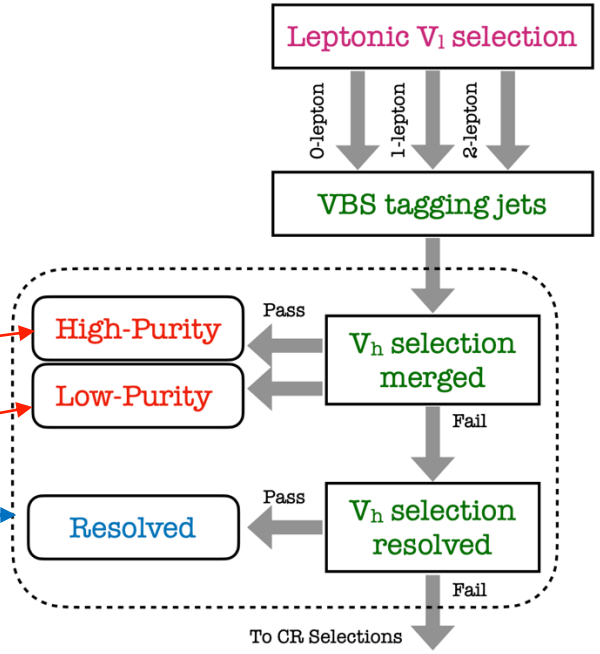

EW diboson production in semileptonic final states at 13 TeV

(arXiv: 2503.17461)

Machine learning approach for final discriminant

A ***Recurrent Neural Network*** **(RNN)** has been developed to separate VBS signal from backgrounds:

- Dedicated training in each channel (0,1,2 leptons) and merged/resolved regions (3x3 SR):
- **Low level input jet variables** for training: $P_T, \eta, \phi, E, n_{tracks}$
- **RNN score used as final discriminant**

9 SR and 9 CR for V+jets and top background

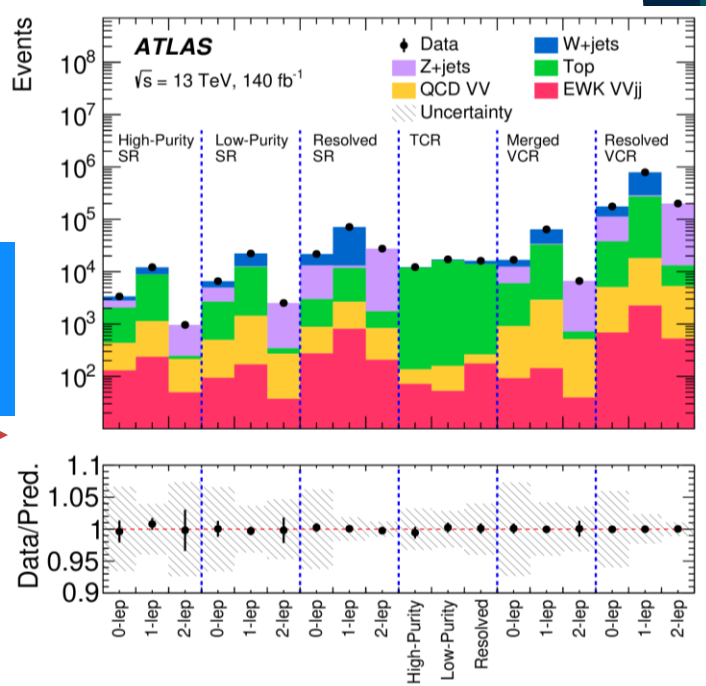

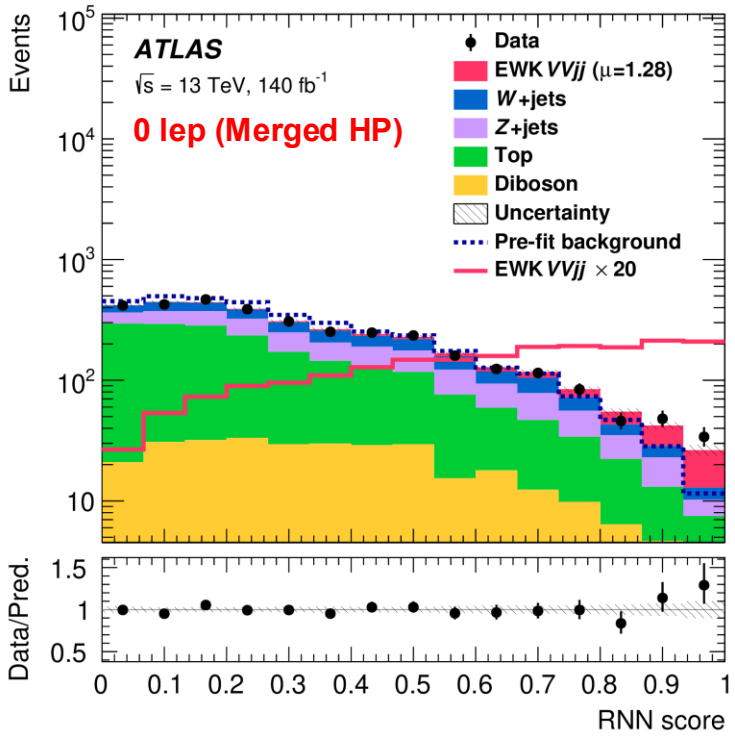

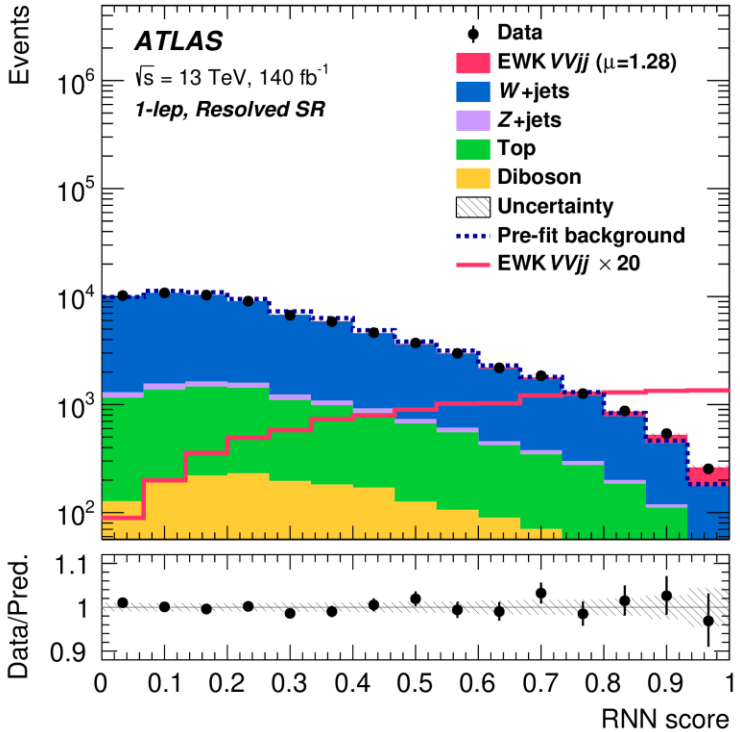

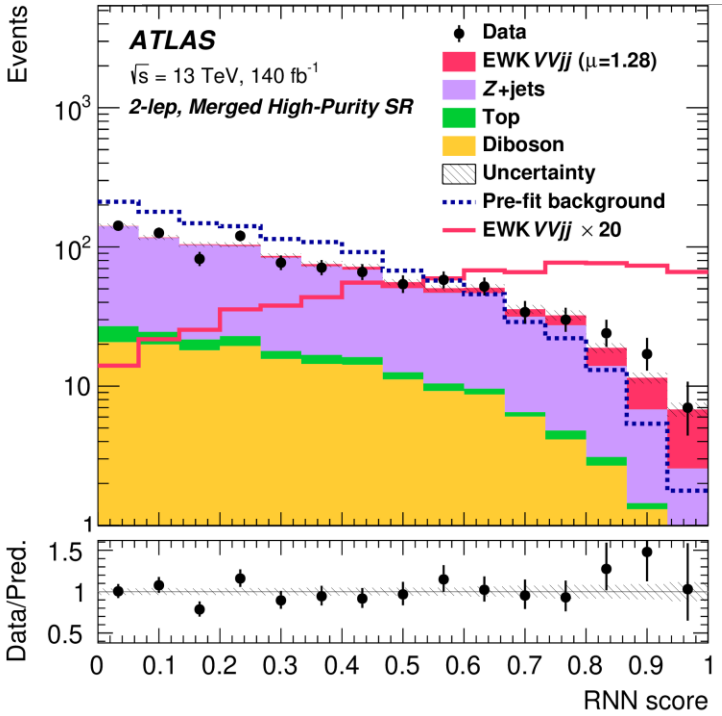

EW diboson production in semileptonic final states at 13 TeV

EW VVjj signal obs. (exp.) significance of **7.4** (6.1) σ

- Measured EW $VVjj$ signal strength:

$$\mu_{\mathrm{EW}}^{\mathrm{obs}} = 1.28^{+0.23}_{-0.21} = 1.28 \pm 0.09\,(\mathrm{stat.})\,^{+0.20}_{-0.19}\,(\mathrm{syst.})$$

Dominated by signal modelling and jet energy calibration uncertainties

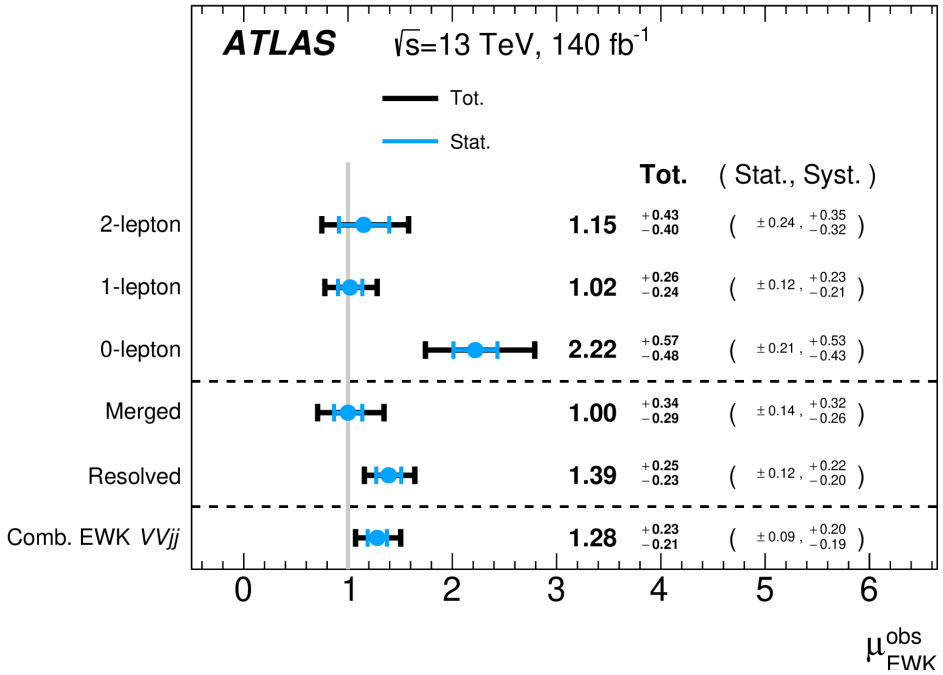

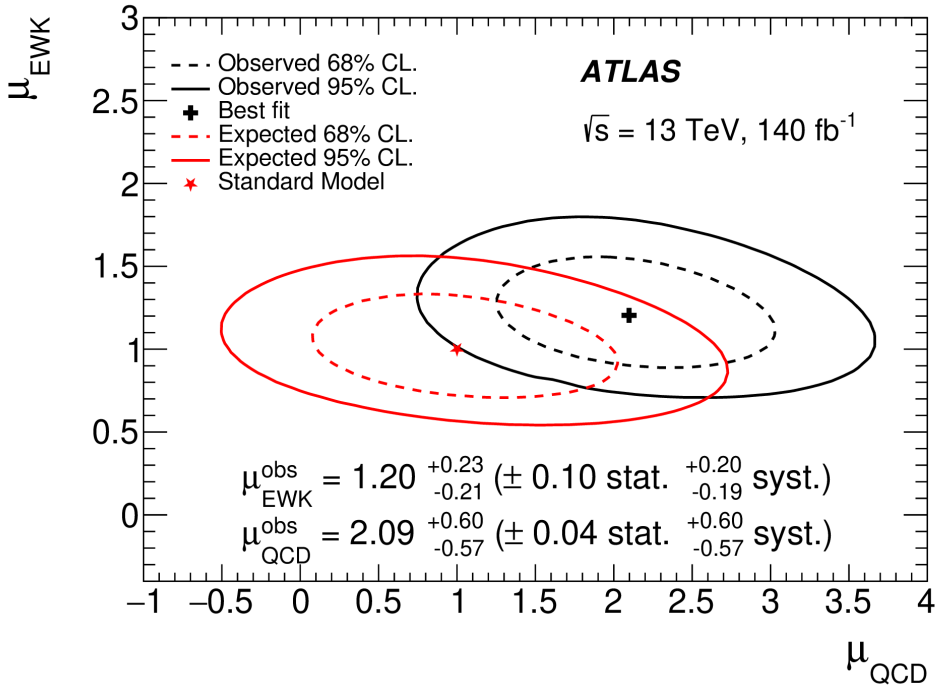

Simultaneously constrain both of EWK and QCD contributions

Fiducial Cross Sections:

	Combined	0-lepton	1-lepton	2-lepton	Resolved	Merged
$\sigma_{EWK}^{\mathrm{fid,exp}}$	20.4 ± 3.5 fb	7.3 ± 2.5 fb	10.3 ± 2.5 fb	2.8 ± 1.1 fb	11.7 ± 3.4 fb	8.7 ± 2.5 fb
$\sigma_{EWK}^{\mathrm{fid,obs}}$	29.2 ± 4.9 fb	15.7 ± 2.8 fb	10.7 ± 2.8 fb	3.1 ± 1.1 fb	17.9 ± 4.3 fb	11.4 ± 3.4 fb

Consistent with the SM

EW diboson production in semileptonic final states at 13 TeV

(arXiv: 2503.17461)

Anomalous quartic gauge coupling (aQGC) effects can be parameterised in the EFT framework

$$\left| A_{\mathrm{SM}} + \sum_i \frac{f_i}{\Lambda^4} A_i \right|^2 = |A_{\mathrm{SM}}|^2 + \sum_i 2\frac{f_i}{\Lambda^4}\mathrm{Re}(A_{\mathrm{SM}}^* A_i) + \sum_i \frac{f_i^2}{\Lambda^8}|A_i|^2 + \sum_{i\neq j} 2\frac{f_i f_j}{\Lambda^8}\mathrm{Re}(A_i^* A_j)$$

EFT-SM interference EFT term EFT cross term

- New D-8 operators contributing to aQGC would enhance EW VBS production at high m_{VV}
- Similar fit setup, but each SR is further split into 2 high and low m_{VV} bins to improve the sensitivity
- Improved constraints for **all** f_S and f_M operators **as large as a factor 3.8 for f_{M0}!**

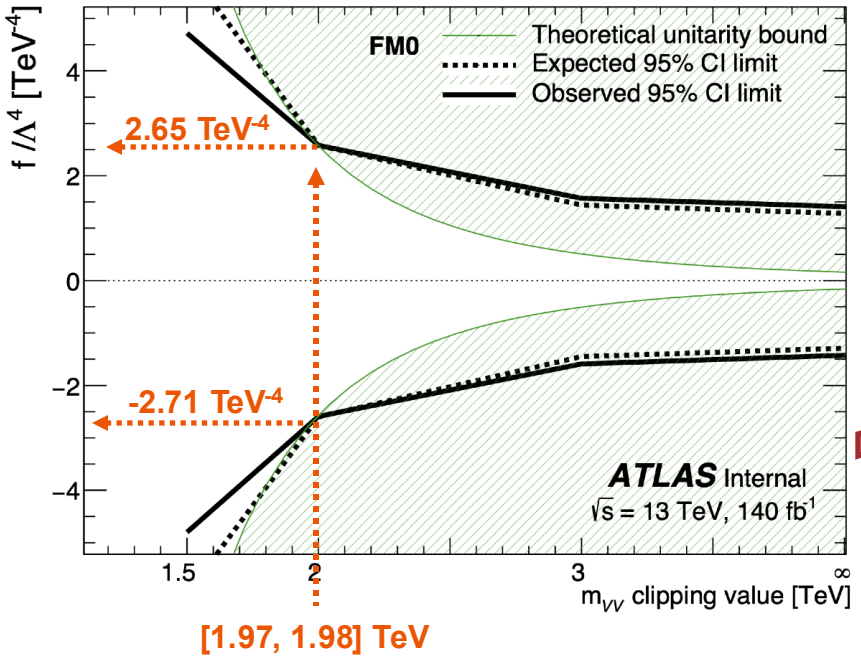

Wilson Coefficient	Expected limit	Observed Limit	Expected Limit Unitarized	Observed Limit Unitarized
f_{T0}/Λ^4	[-0.20, 0.18]	[-0.25, 0.22]	[-0.79, 0.47] at [1.76, 1.96] TeV	[-0.85, 0.47] at [1.73, 2.00] TeV
f_{T1}/Λ^4	[-0.19, 0.19]	[-0.24, 0.24]	[-0.34, 0.34] at [2.59, 2.59] TeV	[-0.43, 0.43] at [2.43, 2.43] TeV
f_{T2}/Λ^4	[-0.44, 0.44]	[-0.55, 0.55]	[-0.95, 0.96] at [2.22, 2.22] TeV	[-1.16, 1.17] at [2.12, 2.11] TeV
f_{T3}/Λ^4	[-0.38, 0.38]	[-0.48, 0.48]	[-0.62, 0.62] at [2.71, 2.71] TeV	[-0.88, 0.88] at [2.49, 2.48] TeV
f_{T4}/Λ^4	[-1.46, 1.32]	[-1.51, 1.37]	[-3.03, 2.60] at [2.02, 2.09] TeV	[-3.03, 2.60] at [2.02, 2.10] TeV
f_{T5}/Λ^4	[-0.57, 0.53]	[-0.64, 0.58]	-	[-2.65, 2.57] at [1.53, 1.54] TeV
f_{T6}/Λ^4	[-0.76, 0.72]	[-0.74, 0.71]	[-2.82, 2.01] at [1.66, 1.73] TeV	[-2.98, 2.62] at [1.64, 1.69] TeV
f_{T7}/Λ^4	[-1.78, 1.52]	[-1.94, 1.70]	[-7.88, 4.29] at [1.65, 1.90] TeV	[-6.70, 4.11] at [1.72, 1.91] TeV
f_{T8}/Λ^4	[-0.59, 0.59]	[-0.48, 0.48]	-	-
f_{T9}/Λ^4	[-1.22, 1.22]	[-1.02, 1.03]	-	-
f_{S02}/Λ^4	[-3.22, 3.22]	[-3.96, 3.96]	[-5.53, 5.54] at [2.07, 2.67] TeV	[-6.16, 6.17] at [2.01, 2.01] TeV
f_{S1}/Λ^4	[-6.84, 6.86]	[-8.06, 8.06]	-	-
f_{M0}/Λ^4	[-1.13, 1.12]	[-1.26, 1.25]	[-2.61, 2.58] at [2.00, 2.00] TeV	[-2.71, 2.65] at [1.97, 1.98] TeV
f_{M1}/Λ^4	[-3.23, 3.24]	[-3.95, 3.95]	[-6.22, 6.22] at [2.27, 2.27] TeV	[-7.42, 7.43] at [2.17, 2.17] TeV
f_{M2}/Λ^4	[-1.66, 1.67]	[-1.85, 1.85]	-	-
f_{M3}/Λ^4	[-5.29, 5.29]	[-5.68, 5.71]	[-23.69, 23.39] at [1.57, 1.57] TeV	[-18.62, 19.10] at [1.66, 1.65] TeV
f_{M4}/Λ^4	[-2.62, 2.62]	[-2.96, 2.97]	-	-
f_{M5}/Λ^4	[-3.81, 3.82]	[-4.41, 4.44]	[-6.80, 6.80] at [2.33, 2.33] TeV	[-7.28, 7.30] at [2.29, 2.29] TeV
f_{M7}/Λ^4	[-5.32, 5.20]	[-6.60, 6.43]	[-9.47, 9.38] at [2.43, 2.43] TeV	[-11.91, 11.11] at [2.29, 2.33] TeV

Importance of Diboson polarization

Study of diboson polarization probes gauge symmetry structure and electroweak symmetry breaking mechanism:

- Vector boson gains the longitudinal polarization in the EWK Spontaneous Symmetry Breaking
- The process $W_L^{\pm}W_L^{\pm} \to W_L^{\pm}\ W_L^{\pm}$ would **violate unitarity if Higgs coupling deviates from the SM**
- LHC experiments gaining sensitivity to $V_L\ V_L$ production and starting to study energy dependence of cross-section

W polarization determines decay angle:

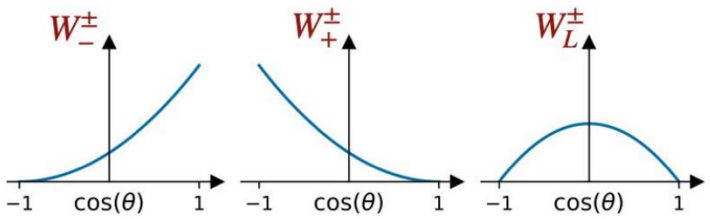

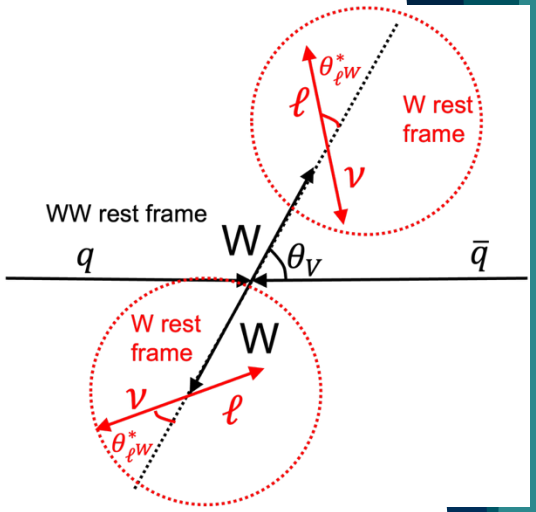

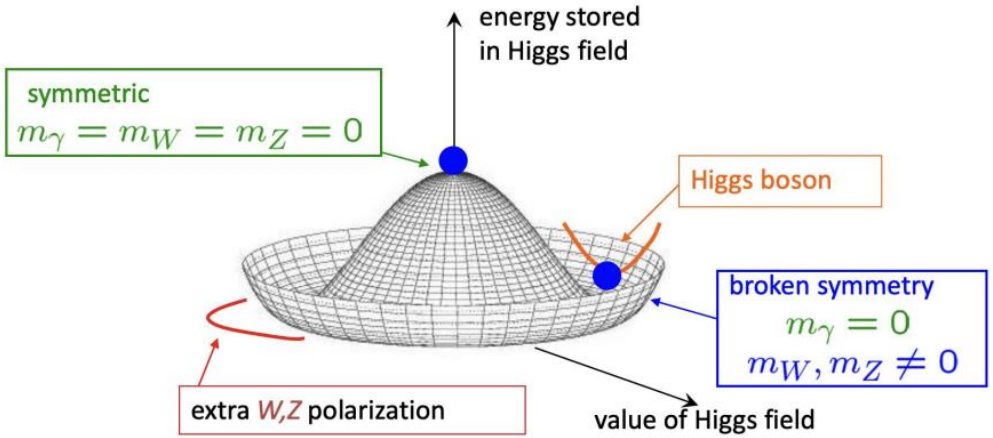

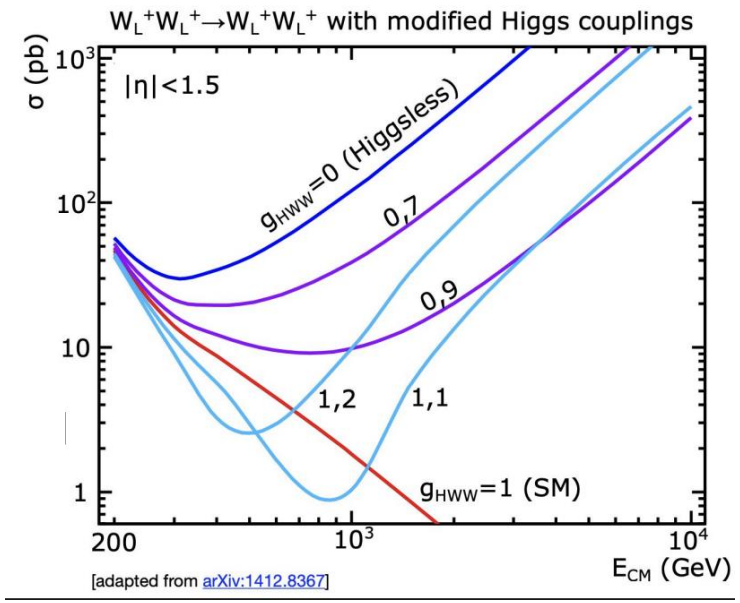

Massless fields interacting with a complex weak isospin doublet can spontaneously break EW symmetry and generate W and Z masses

The process would violate unitarity if Higgs coupling deviates from the SM ⇒ **is a unique opportunity to probe electroweak symmetry**

Boson Polarization in VBS (WW same sign)

arXiv:2503.11317

First ATLAS observation

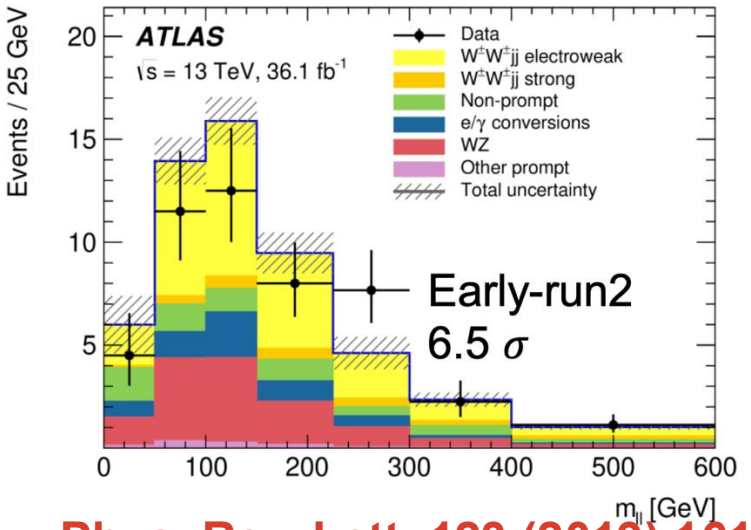

Phys. Rev. Lett. 123 (2019) 161801

W polarization determines decay angle

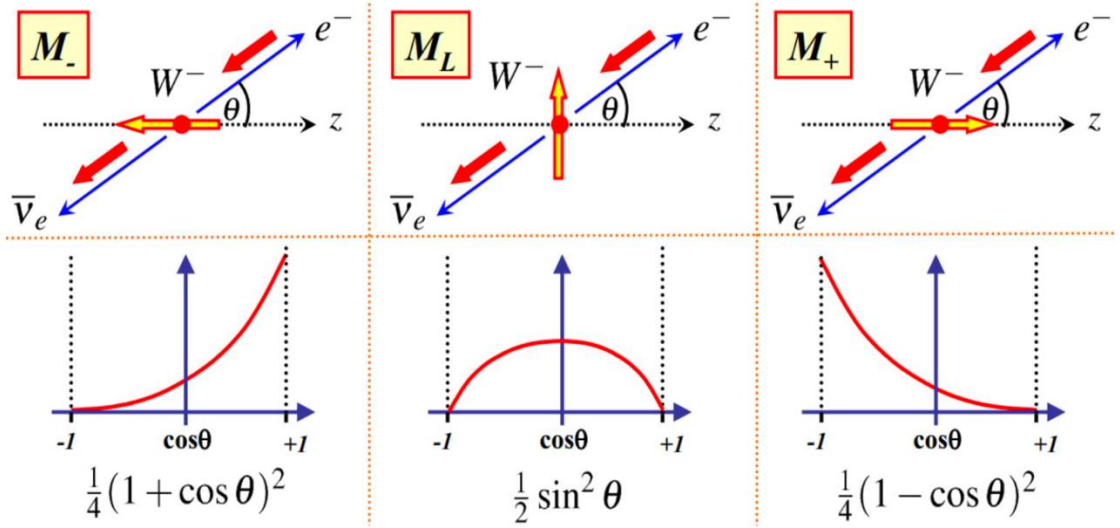

NEW March 2025!!!

Feynman diagrams for a VBS EW $W^{\pm}W^{\pm}jj$ production

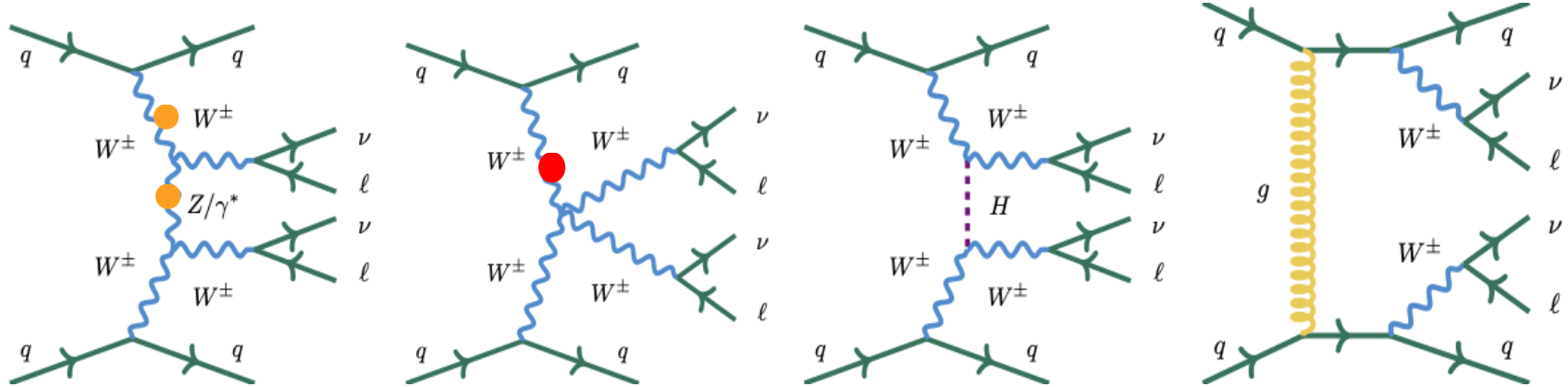

triple-gauge boson vertices

quartic gauge boson vertex

exchange of a Higgs boson

QCD $W^{\pm}W^{\pm}jj$ production

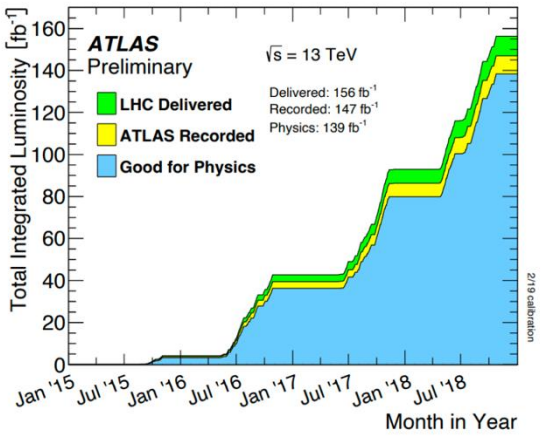

EW $W^{\pm}W^{\pm}$ production via VBS

Boson Polarization in VBS (WW same sign)

arXiv:2503.11317

LHC Full-run2 data, $\mathcal{L}$ = 140.1 ± 1.2 fb−1
Electroweak $W^{\pm}W^{\pm}jj \rightarrow lvlvjj, l = e, \mu$

Search for the longitudinal polarization mode and measure the cross-section

- $W_L W_L$: search for di-longitudinal mode
- $W_L W$: search for longitudinal mode

Polarization defined in WW-COM frame

- LL has relatively higher fraction in WW-COM

Signal: EWK $W\pm W\pm jj \rightarrow lvlvjj$ $(\mathcal{O}(\alpha^6))$ (Sherpa3)

Background:

$W^{\pm}W^{\pm}jj$ backgrounds: MG+Herwig7

- QCD $(\mathcal{O}(\alpha^4\alpha_s^2))$
- QCD-EWK interference $(\mathcal{O}(\alpha^5\alpha_s))$

$WZjj$ backgrounds: Sherpa 2.2.12

- QCD $(\mathcal{O}(\alpha^4\alpha_s^2))$
- EWK interference $(\mathcal{O}(\alpha^6))$

Other prompt (ZZjj, Z+jets , tt, ttV , Vγ)

Non-prompt background (W+jets, Top), charge misID and photon conversion

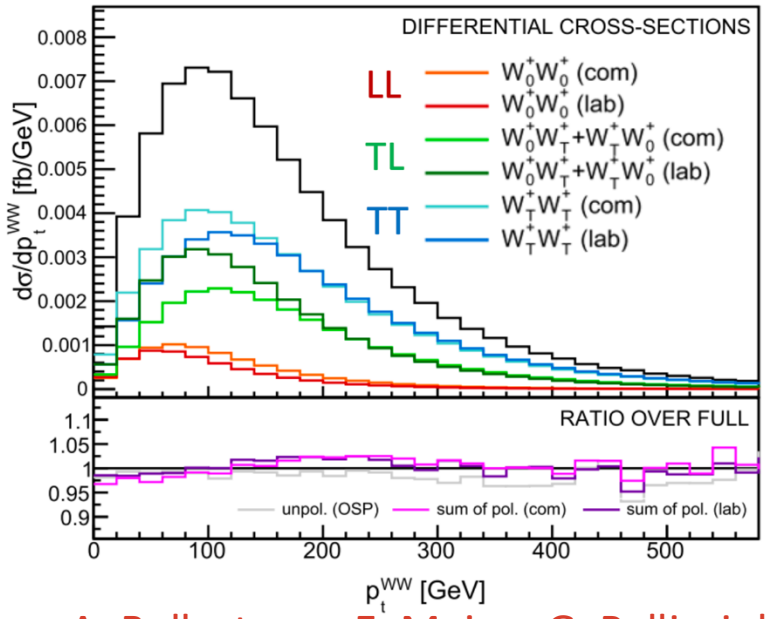

A. Ballestrero, E. Maina, G. Pelliccioli

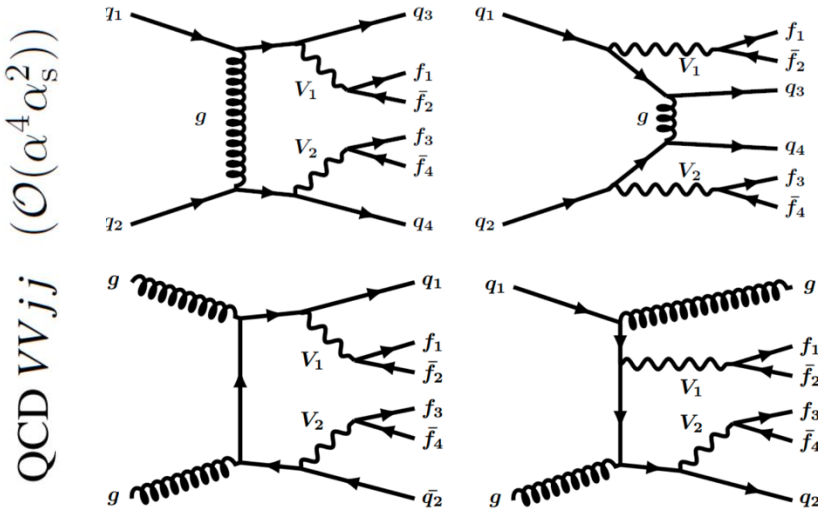

Boson Polarization in VBS (WW same sign)

arXiv:2503.11317

- Standard VBS selection procedure: 2 forward jets with large rapidity gap and large invariant mass plus 2 same sign **leptons** (see: JHEP 04 (2024) 026)
- Updated with state-of-art Sherpa3 polarisation modelling with NLO EW & QCD corrections
- Polarization mode now reflects in the kinematics of leptons and jets → DNN approach:
  - **DNN$_{\text{inclusive}}$**: separate EW $W^{\pm}W^{\pm}jj$ from background
  - **DNN$_{\text{signal}}$**: separate $W_L^{\pm}W_L^{\pm}$ vs $W_T^{\pm}W_X^{\pm}$ (with X=L,T)
  - **DNN$_{\text{signal}}$**: separate $W_L^{\pm}W_X^{\pm}$ vs $W_T^{\pm}W_T^{\pm}$

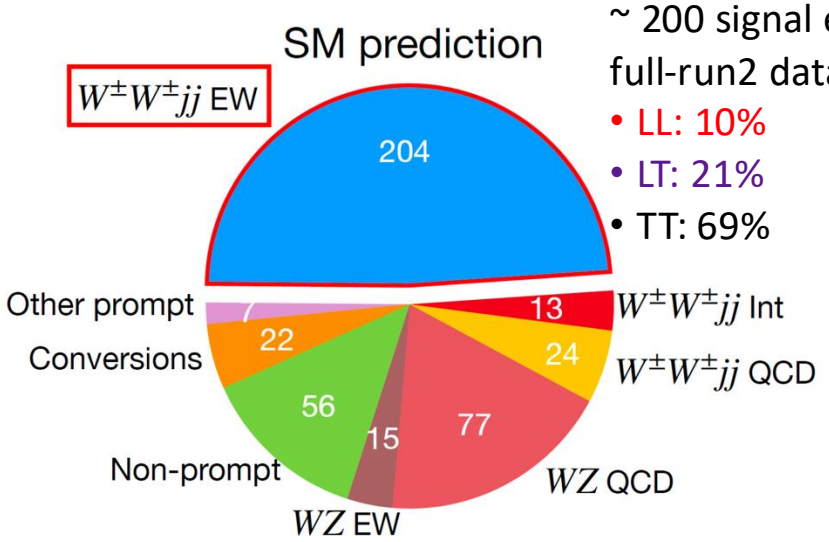

~ 200 signal events in full-run2 data:
- LL: 10%
- LT: 21%
- TT: 69%

- DNNs trained with up to 20 input variables such as $\Delta\eta_{\ell\ell}$, $m_{\ell\ell}$, $\Delta\phi_{jj}$, m_{jj}, m_T^0, $m_T^{\ell_2}$, $p_T^{j_i}$, … DNN$_{\text{polarization}}$

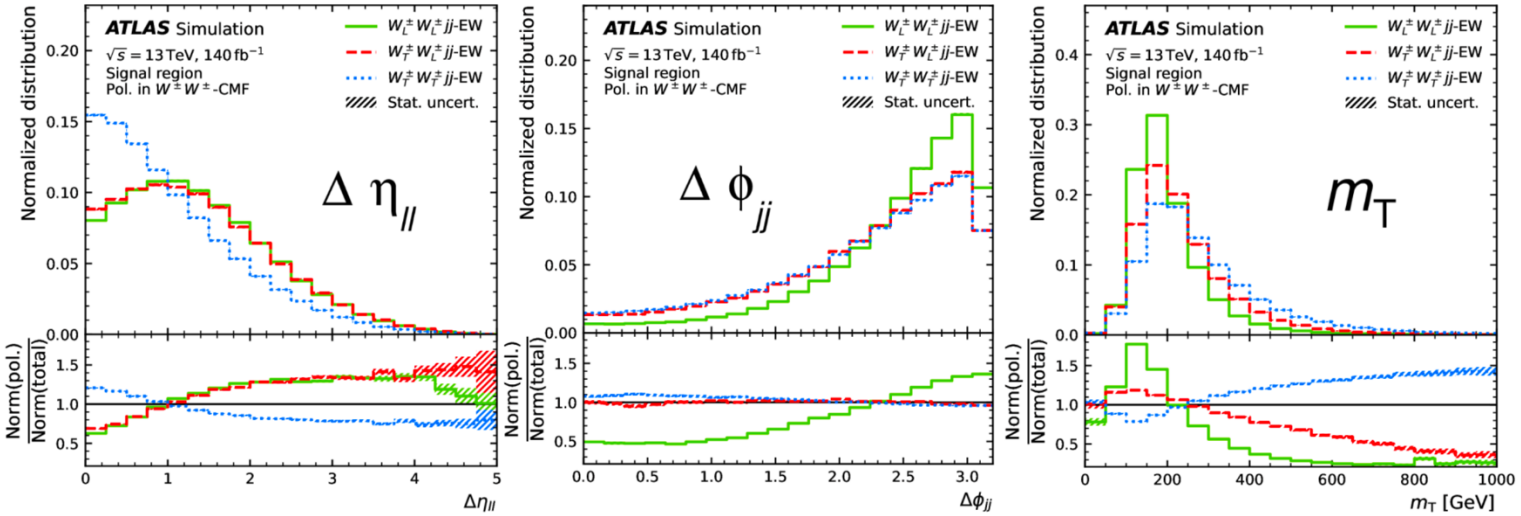

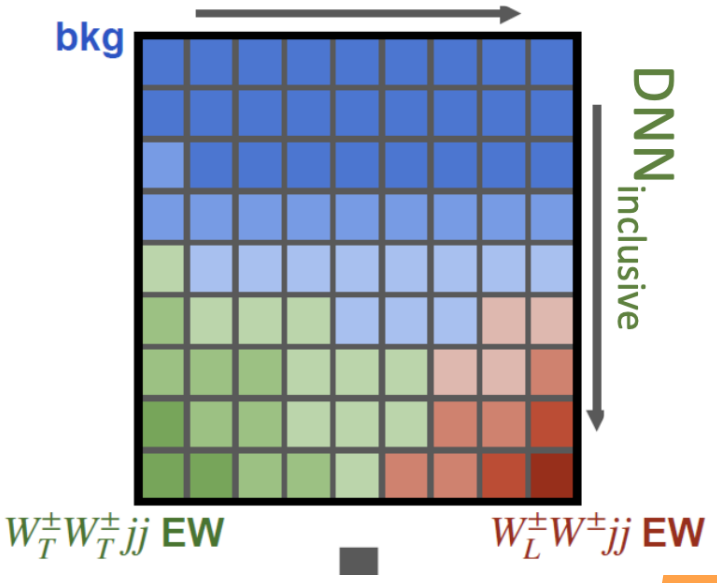

Same-sign W boson polarisation

- Binned maximum-likelihood fits performed to extract the $W_L^{\pm}W_L^{\pm}$ and $W_L^{\pm}W_X^{\pm}$ signal strength
- Fit performed in **3 regions** of **$DNN_{inclusive}$**
- Each **$DNN_{inclusive}$** region contains 3-6 **DNNpolarization** bins
- A **low- m_{jj}** and WZ CRs also enter the fit

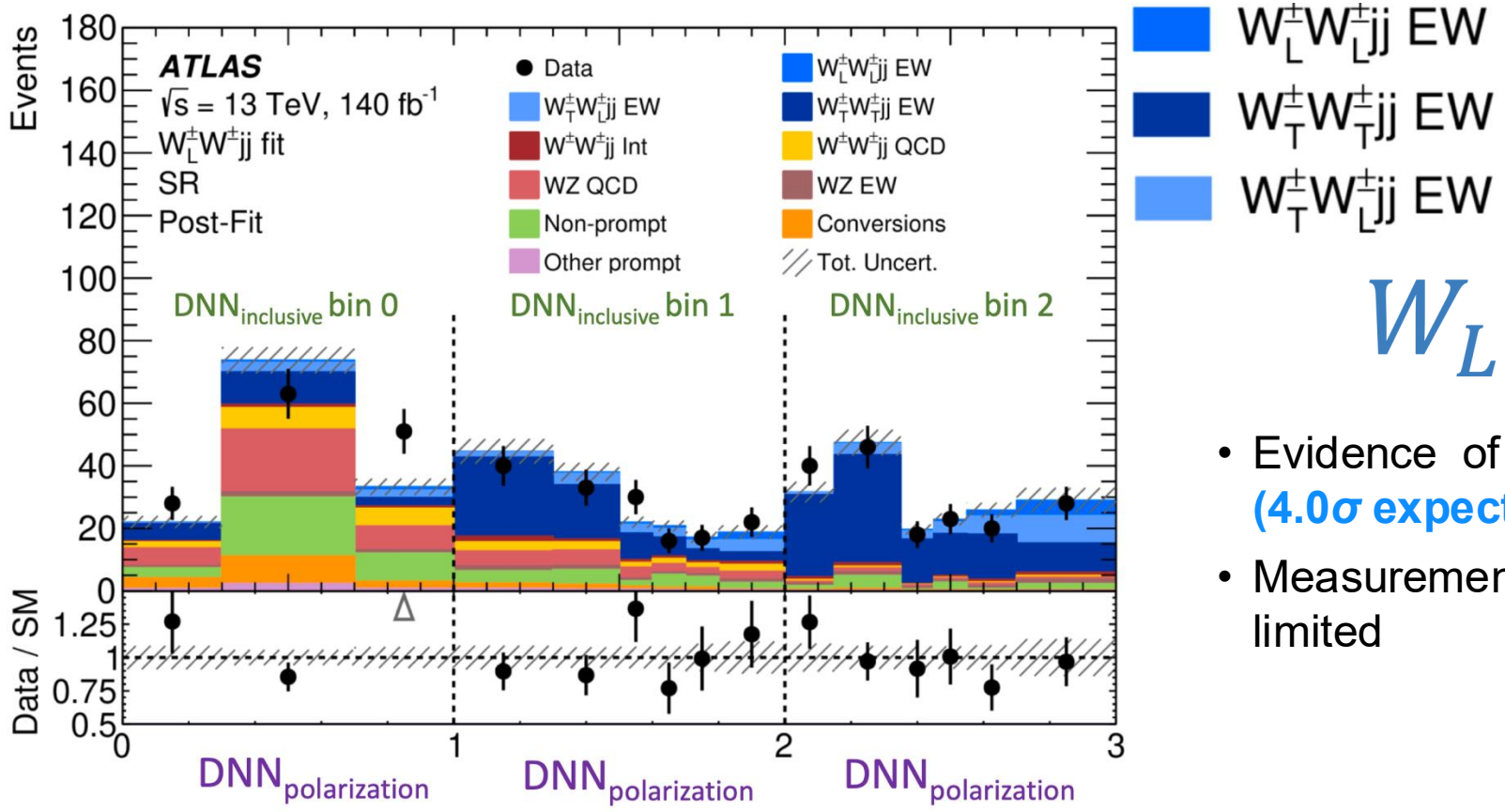

Source of uncertainty	Impact [%]
Experimental	
Lepton calibration	0.2
Jet energy and E_T^{miss} scale and resolution	3.9
Pileup modelling	1.2
Background, misid. leptons	4.2
Background, charge misrec.	0.5
Luminosity	1.1
Modeling	
$W^{\pm}W^{\pm}jj$ EW + QCD uncertainties	4.7
Background, WZ scale, PDFs & α_s	0.4
Background, WZ reweighting	0.3
Model statistical	7.2
Small background normalizations	1.1
Normalisation factors	2.5
Experimental and modelling	11.1
Data statistical	34.1
Total	34.1

$W_L W jj$ results

- Evidence of $W_L^{\pm}W_X^{\pm}$ state: **3.3σ observed (4.0σ expected)**
- Measurement precision is **statistically** limited

Same-sign W boson polarisation

- Binned maximum-likelihood fits performed to extract the $W_L^{\pm}W_L^{\pm}$ and $W_L^{\pm}W_X^{\pm}$ signal strength
- Fit performed in **3 regions** of **DNN$_{inclusive}$**
- Each **DNN$_{inclusive}$** region contains 3-6 **DNNpolarization** bins
- A **low-m_{jj}** and WZ CRs also enter the fit

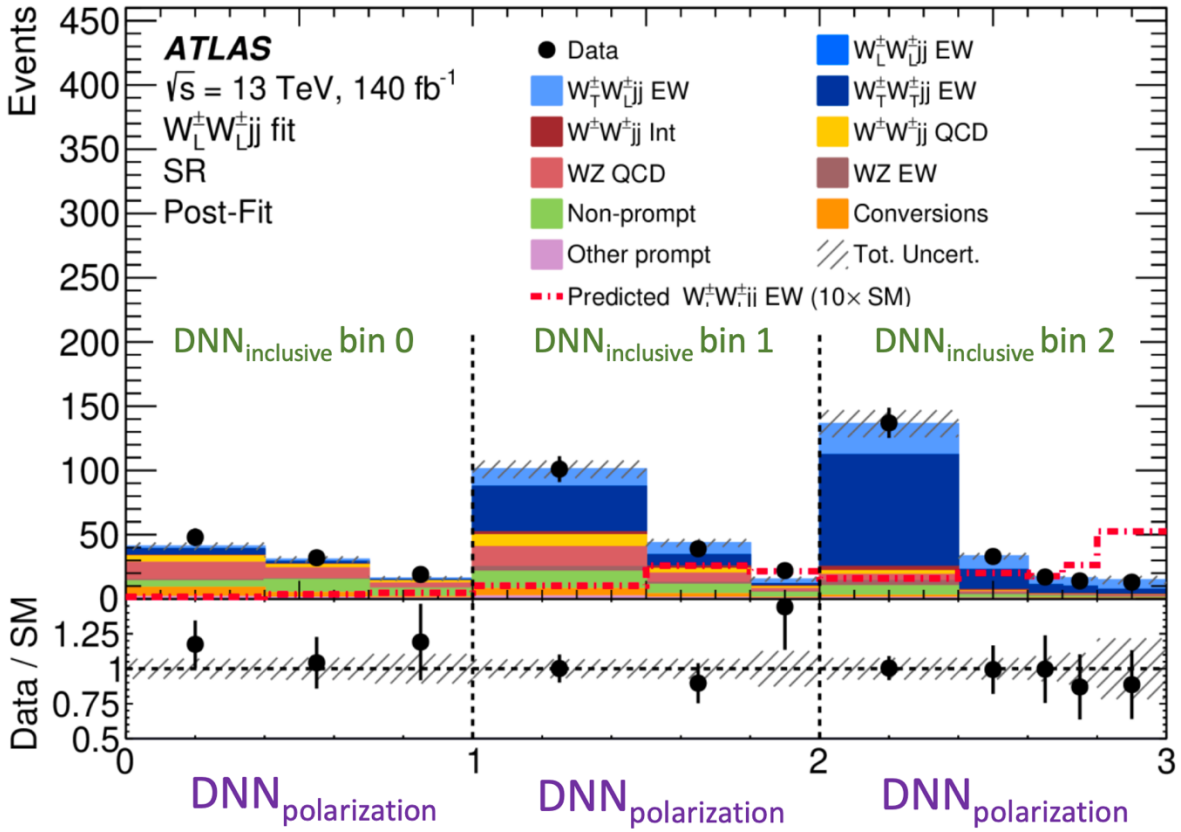

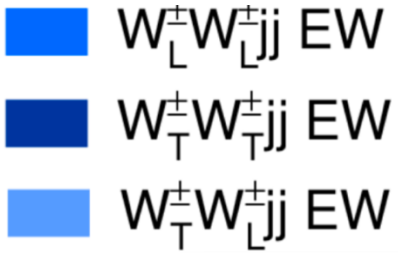

Source of uncertainty	Impact [%]
Experimental	
Lepton calibration	0.2
Jet energy and E_T^{miss} scale and resolution	3.9
Pileup modelling	1.2
Background, misid. leptons	4.2
Background, charge misrec.	0.5
Luminosity	1.1
Modeling	
$W^{\pm}W^{\pm}jj$ EW + QCD uncertainties	4.7
Background, WZ scale, PDFs & α_s	0.4
Background, WZ reweighting	0.3
Model statistical	7.2
Small background normalizations	1.1
Normalisation factors	2.5
Experimental and modelling	11.1
Data statistical	34.1
Total	34.1

$W_L W_L$ results

95% CL upper limit of 0.45 fb (exp. 0.70 fb)

The most stringent limit to data for fully longitudinal polarized $W_L^{\pm}W_L^{\pm}$jj
Dominated by statistical uncertainnty

Same-sign W boson polarisation

- The measured fiducial cross-sections times branching fractions are compared to the theoretical predictions from Sherpa3
- First fixed-order NLO EW corrections for the different $W_L^{\pm}W_L^{\pm}$jj, $W_L^{\pm}W_T^{\pm}$jj and $W_T^{\pm}$ $W_T^{\pm}$jj processes are used (arXiv:2409.03620), reducing by ≈ 15% the cross-section in the SR
- **The measured cross sections are in agreement with the SM predictions**
- Results driven by the statistical uncertainty of the data in the SR

Studies performed in the **WW** and **partonic** centre-of-mass frames (CMF)

WW - CMF

Process	Prediction	Measured $\sigma\mathcal{B}$ (fb)	Uncertainty breakdown (fb)
$W_L^{\pm}W_L^{\pm}jj$	0.29 ± 0.07	0.01 ± 0.21 (tot.)	± 0.20 (stat.) ± 0.05 (mod. syst.) ± 0.02 (exp. syst.)
$W_T^{\pm}W^{\pm}jj$	2.56 ± 0.64	3.39 ± 0.35 (tot.)	± 0.30 (stat.) ± 0.11 (mod. syst.) ± 0.14 (exp. syst.)
$W_L^{\pm}W^{\pm}jj$	1.18 ± 0.29	0.88 ± 0.30 (tot.)	± 0.28 (stat.) ± 0.08 (mod. syst.) ± 0.05 (exp. syst.)
$W_T^{\pm}W_T^{\pm}jj$	1.67 ± 0.40	2.49 ± 0.32 (tot.)	± 0.30 (stat.) ± 0.09 (mod. syst.) ± 0.10 (exp. syst.)

partonic - CMF

Description	Prediction	Measured $\sigma\mathcal{B}$ (fb)	Uncertainty breakdown (fb)
$W_L^{\pm}W_L^{\pm}jj$	0.19 ± 0.05	0.16 ± 0.22 (tot.)	± 0.21 (stat.) ± 0.05 (mod. syst.) ± 0.03 (exp. syst.)
$W_T^{\pm}W^{\pm}jj$	2.67 ± 0.66	3.40 ± 0.35 (tot.)	± 0.31 (stat.) ± 0.11 (mod. syst.) ± 0.14 (exp. syst.)
$W_L^{\pm}W^{\pm}jj$	1.24 ± 0.31	0.84 ± 0.37 (tot.)	± 0.35 (stat.) ± 0.10 (mod. syst.) ± 0.07 (exp. syst.)
$W_T^{\pm}W_T^{\pm}jj$	1.62 ± 0.39	2.46 ± 0.37 (tot.)	± 0.34 (stat.) ± 0.10 (mod. syst.) ± 0.11 (exp. syst.)

Summary & Conclusions

In this talk, recent **ATLAS** results on Vector boson scattering at $\sqrt{s}$ = 13 TeV using 140 fb^{-1} were presented:

- **First observation of EW $VVjj$ production in semileptonic decay**:

7.4σ observed (6.1σ expected)
ML approach based on RNN architecture has been developed to separate VBS signal from backgrounds
Significantly improved limits on anomalous QGCs

- **First evidence for longitudinal polarization in vector boson scattering**:

3.3σ observed (4.0σ expected)
Analysis use state-of-the-art polarization prediction: Multi-jet merging in matrix element and NLO EW correction
Most stringent limits on fully longitudinally polarized $W\pm W\pm jj$ EW production (1.6 $\times$ SM)

Backup

SM rarest processes: VBS and $W^{\pm}W^{\pm}$

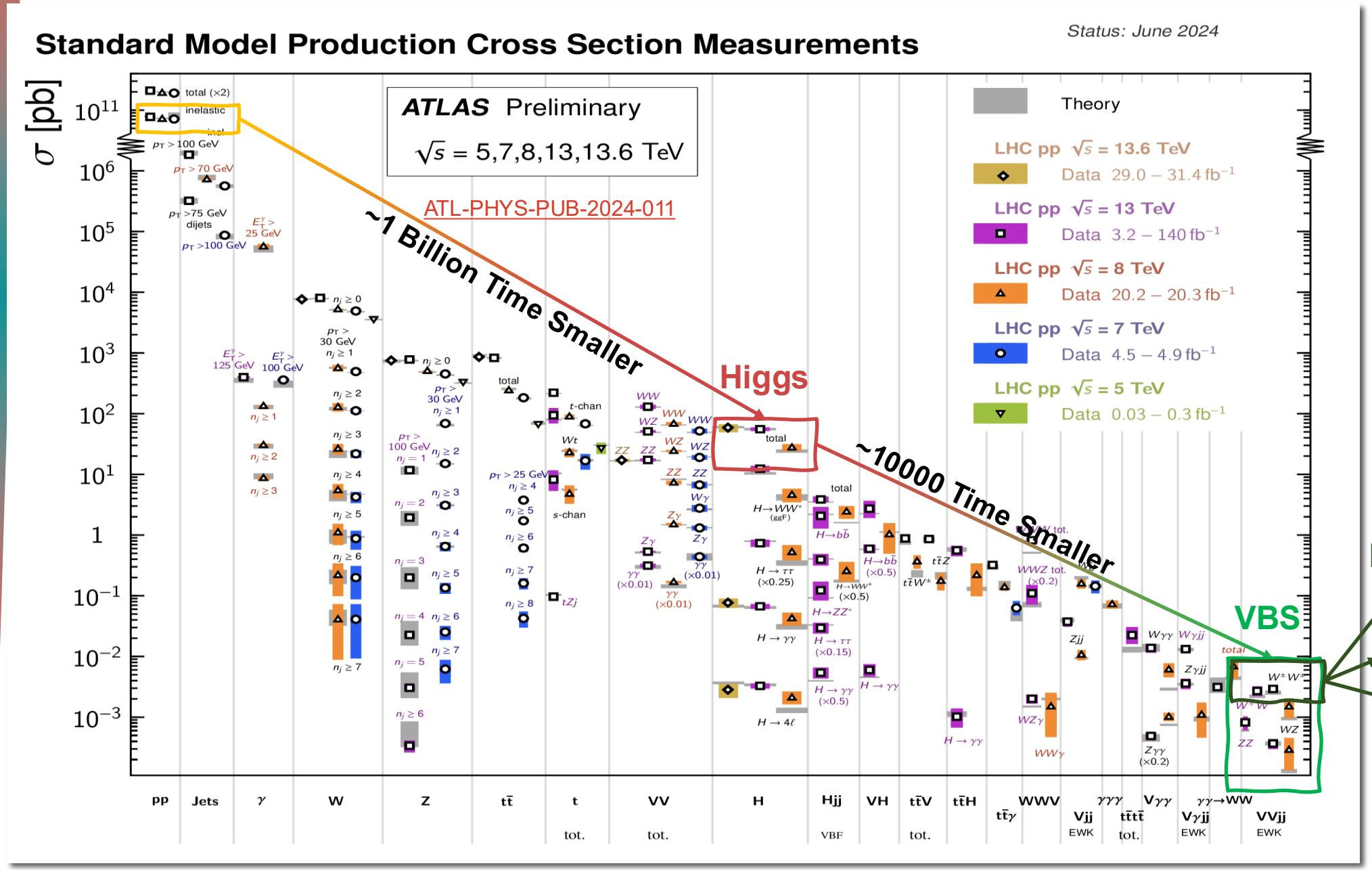

Extremely Rare!

Expected fractions:

61% $W_T^{\pm}W_T^{\pm}$

29% $W_T^{\pm}W_L^{\pm}$

10% $W_L^{\pm}W_L^{\pm}$

39% $W_L^{\pm}W_L^{\pm}$

MC samples for VBS semileptonic

EWK signal samples: MadGraph5_aMC@NLO 2.6.6, NNPDF3.0nlo PDF set, parton shower and hadronization with Pythia 8.186
EFT samples: MadGraph5_aMC@NLO v2.7.2, NNPDF3.0nlo PDF set, parton shower and hadronization with Pythia 8.244

QCD VVjj: SHERPA2.2.1, NNPDF3.0nlo PDF set, xsec @ NLO
V+jets: SHERPA2.2.1, xsection @ NNLO
tt, single-top: Powheg Box v2 generator at NLO, NNPDF3.0nlo PDF set. Xsection is NNLO for tt and NLO for single t. Both have NNLL resummation of soft-gluon terms

Polarization simulation

Polarization mode of W boson can not be directly extracted from the decay angle due to neutrinos in the final state:

- Reflected in the kinematics of leptons, jets and missing energies.
- Precise full-kinematics simulation is essential

NLO QCD + NLO EW together modifies the $W\pm W\pm jj$ by 15- 30%,

- different impact to polarization modes
- Absence of NLO simulation can lead to an uncertainty > 20%

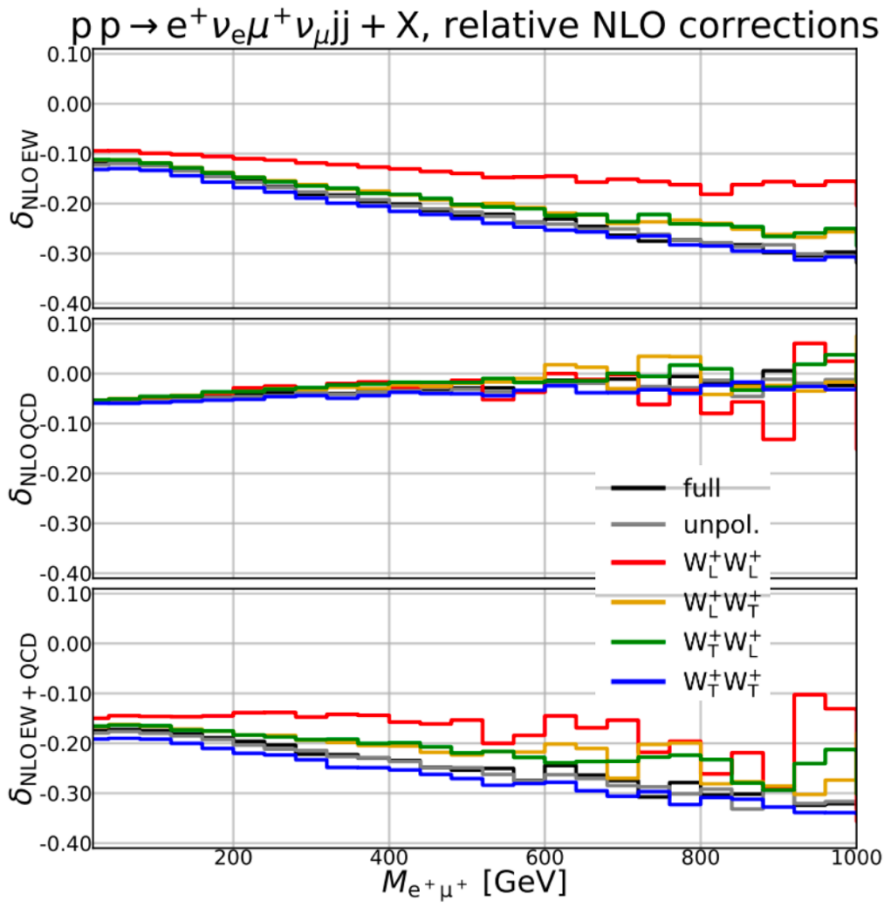

A. Denner ,C. Haitz, G. Pelliccioli

Sherpa3 provides VBS polarization simulation for:

- LL, TL, TT and polarization Interference
- LO in EW and approximate NLO in pQCD
- NLO EW correction from A. Denner ,C. Haitz, G. Pelliccioli

Same-sign W boson polarisation (Input variables with data)

- Measurement of production cross sections of polarised at with $W^{\pm}W^{\pm}$ at 13 TeV with 140 fb^{-1}
- Based on Run 2 cross-section measurement 2312.00420
- Updated with state-of-art Sherpa3 polarisation modelling with NLO EW & QCD corrections
- Frame dependant measurement using Deep Neural Networks built for:
  - DNN$_{\text{inclusive}}$: separate EW $W^{\pm}W^{\pm}jj$ from background
  - LL - DNN$_{\text{signal}}$: separate $W_L^{\pm}W_L^{\pm}$ vs $W_T^{\pm}W_X^{\pm}$ (with X=L,T)
  - LX - DNN$_{\text{signal}}$: separate $W_L^{\pm}W_X^{\pm}$ vs $W_T^{\pm}W_T^{\pm}$
- DNNs trained with up to 20 input variables such as $\Delta\eta_{\ell\ell}$, $m_{\ell\ell}$, $\Delta\phi_{jj}$, m_{jj}, m_T^0, $m_T^{\ell_2}$, $p_T^{j_i}$, …

Higher-ranked variables

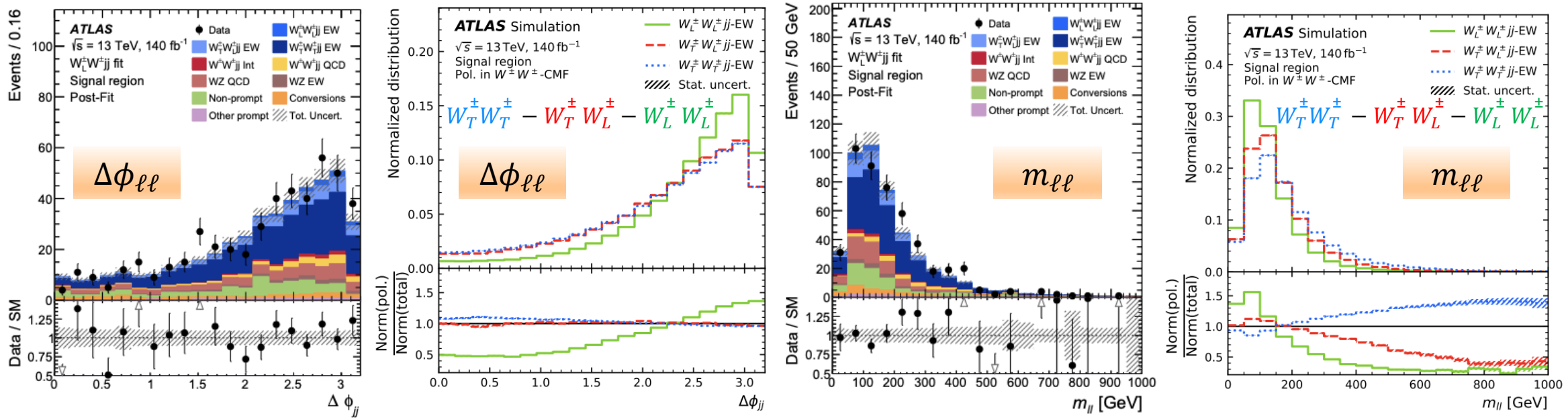

Fiducial region

Fiducial region definition for $W_L W_L$

- Events with taus from W decays in the ME calculation are vetoed. They constitute around 15% of the SR cross section;
- Two prompt leptons (e or μ) with p_T> 27 GeV and $|\eta| < 2.5$ dressed with prompt photons within a $\Delta R < 0.1$.
- The two leptons must have same sign electric charge and have the invariant mass $m_{\ell\ell}$> 20 GeV;
- At least two jets from the `AntiKt4TruthJets` container with p_T>65 GeV for the leading and p_T>35 GeV for the sub-leading jet, and $|\eta|$<4.5, reconstructed with the anti-kt algorithm with radius parameter R = 0.4;
- Truth overlap removal. The `AntiKt4TruthJets` container is used to access truth jet information in `DAOD_STDM3` samples. The jets in this container are clustered excluding neutrinos and muons, but including electrons, to match the detector level definitions of jets [53]. Therefore, an additional step of overlap removal between electrons and jets is needed. The adopted procedure is the following. If an electron and a jet overlap with $\Delta R(e, \text{jet}) < 0.4$, and the ratio $p_{T,e}/p_{T,\text{jet}} < 0.5$, then the electron is assumed to come from a hadron decay within the jet and is removed. If $p_{T,e}/p_{T,\text{jet}} > 0.5$, then most of the time the jet contains a single particle – electron, and is therefore removed. No overlap removal between muons and jets is applied;
- Z veto in the ee channel: ee events with the dielectron invariant mass in the range $|m_{ee} - m_Z| < 15$ GeV are removed;
- The truth-level MET as reconstructed from the visible final state objects passing the above selections must satisfy the condition $E_T^{\text{miss}} > 30$ GeV;
- The invariant mass of the two highest-p_T jets must be m_{jj} >500 GeV;
- The separation in rapidity between the two highest-p_T jets has to be $\Delta Y(j, j)$>2.0.

Diboson and multibosons as Electroweak Tests at LHC

LHC as a precision machine: diagrams in which two ore more Vector Boson interacts, giving either one or two Vector Bosons in the final state, are among the rarest and more challenging processes measured

Investigation of EW gauge structure

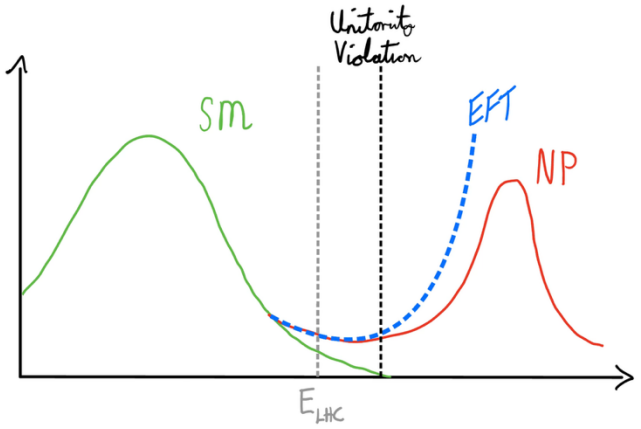

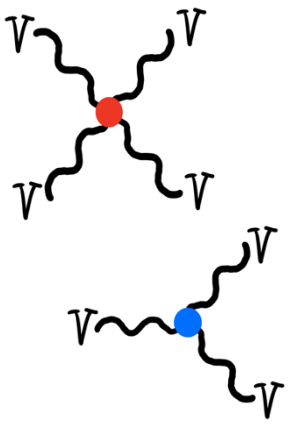

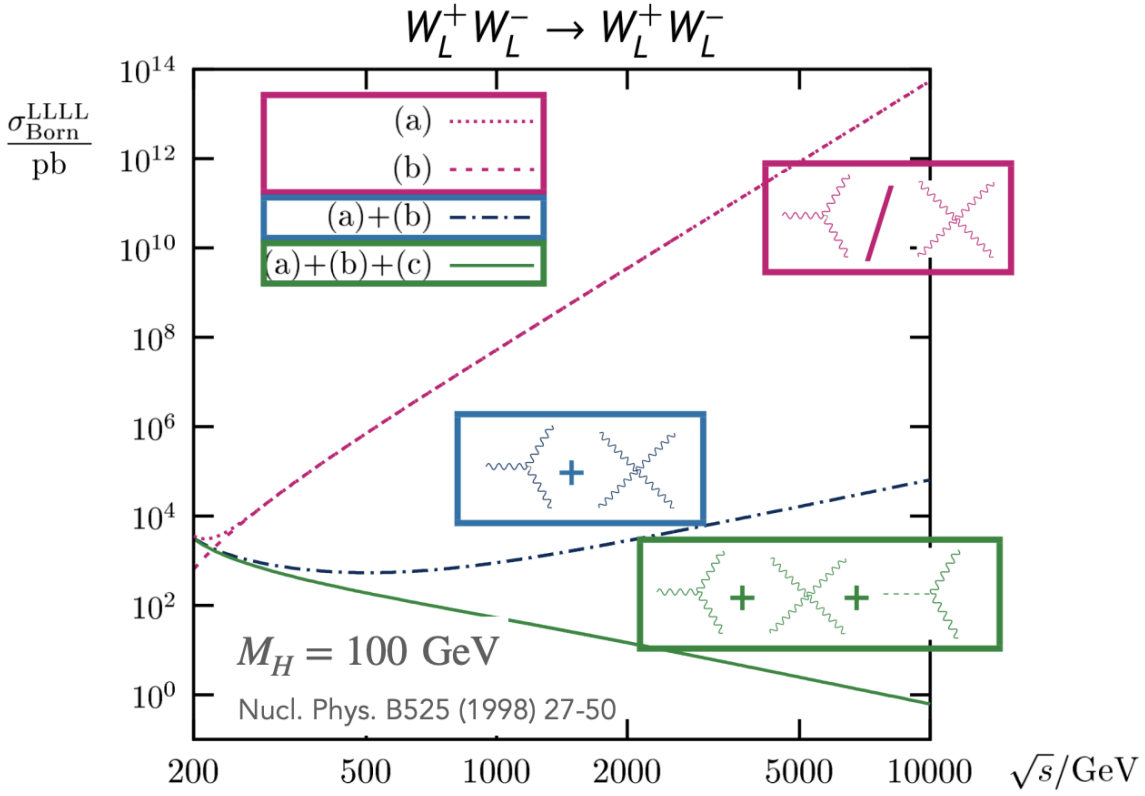

Effective field theory (EFT) interpretation:

$$\mathcal{L}_{SMEFT} \approx \mathcal{L}_{SM}^{(4)} + \sum_i \frac{c_i^{(6)}}{\Lambda^2} \mathcal{O}_i^{(6)} + \sum_i \frac{c_i^{(8)}}{\Lambda^8} \mathcal{O}_i^{(8)}$$

$\mathcal{O}_i^{(6)}$: dim-6 EFT operators invariant under SM suppressed by powers of Λ^2

$\mathcal{O}_i^{(8)}$: dim-8 EFT operators invariant under SM suppressed by powers of Λ^4

- Must ensure perturbative unitarity is not violated by checking against theoretical bounds
- Use clipping scan where EFT effects are turned off above a range of parameters

- Delicate gauge cancellations at high energy
- Enhanced sensitivity to non-SM contributions

Same-sign W boson polarisation

- $\Delta\eta_{\ell\ell}, m_{\ell\ell}, \Delta\phi_{jj}, m_{jj}, m_T^{\mathrm{O}}, m_T^{\ell_2}, p_T^{j_i}, \ldots$

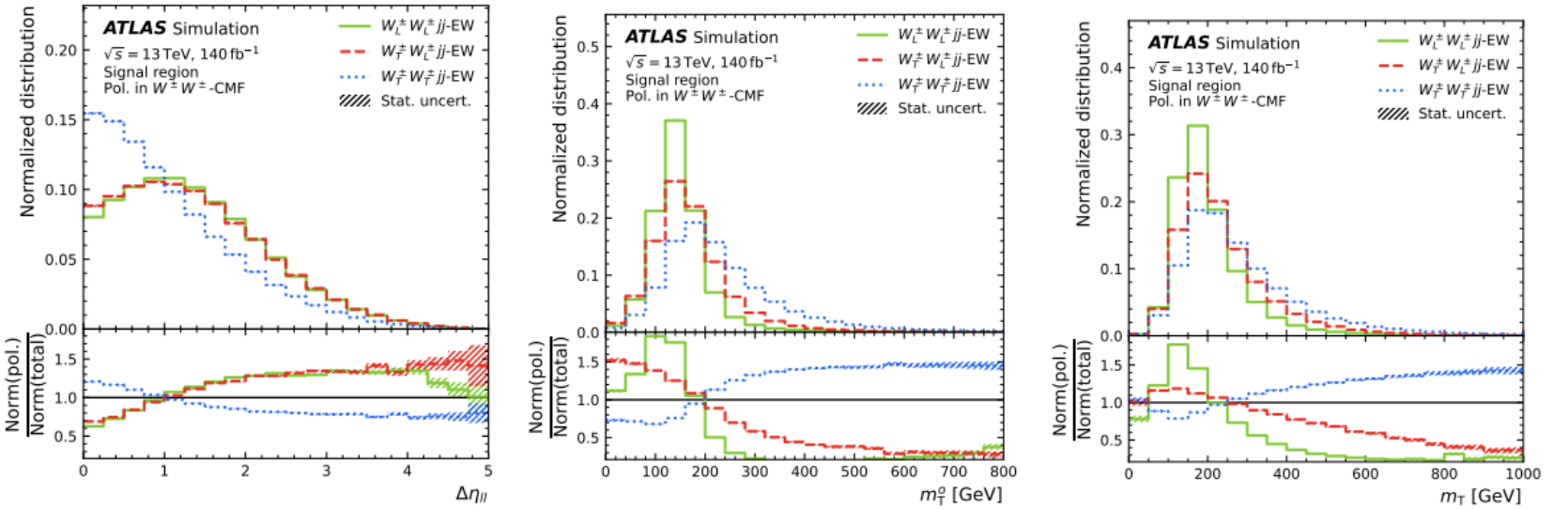

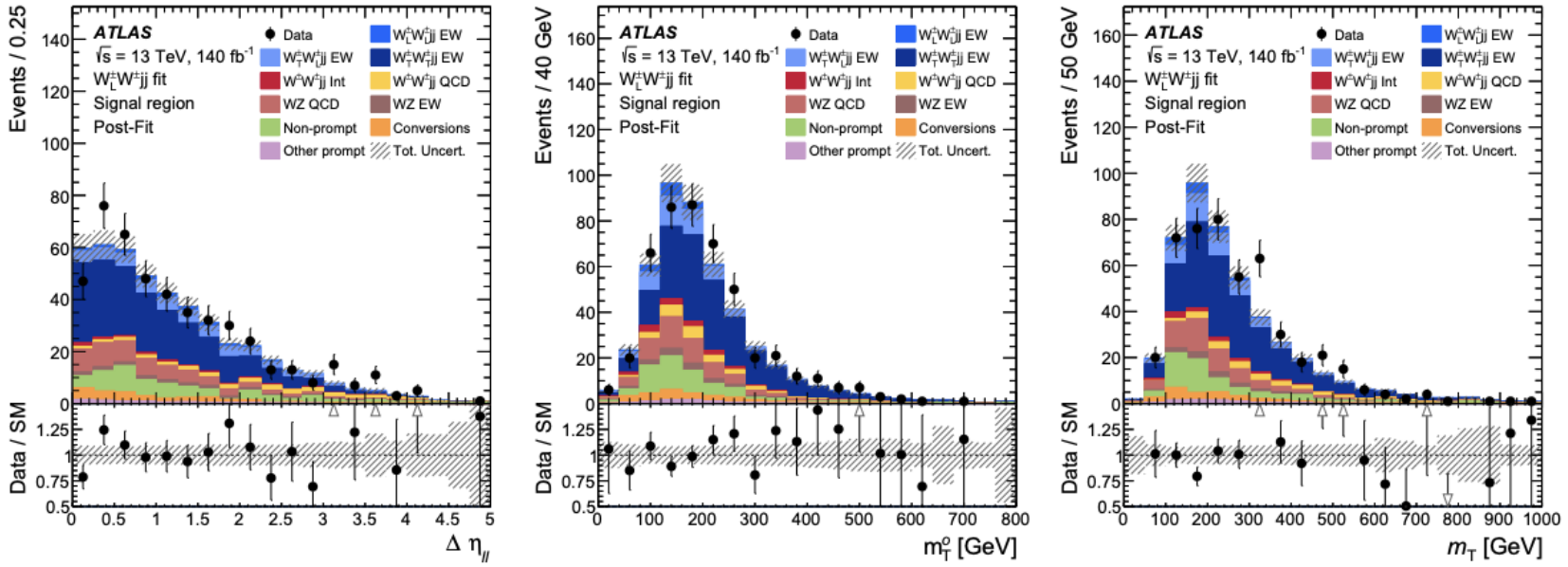

Same-sign W boson polarisation

- $\Delta\eta_{\ell\ell}, m_{\ell\ell}, \Delta\phi_{jj}, m_{jj}, m_T^{\mathrm{O}}, m_T^{\ell_2}, p_T^{j_i}, \ldots$

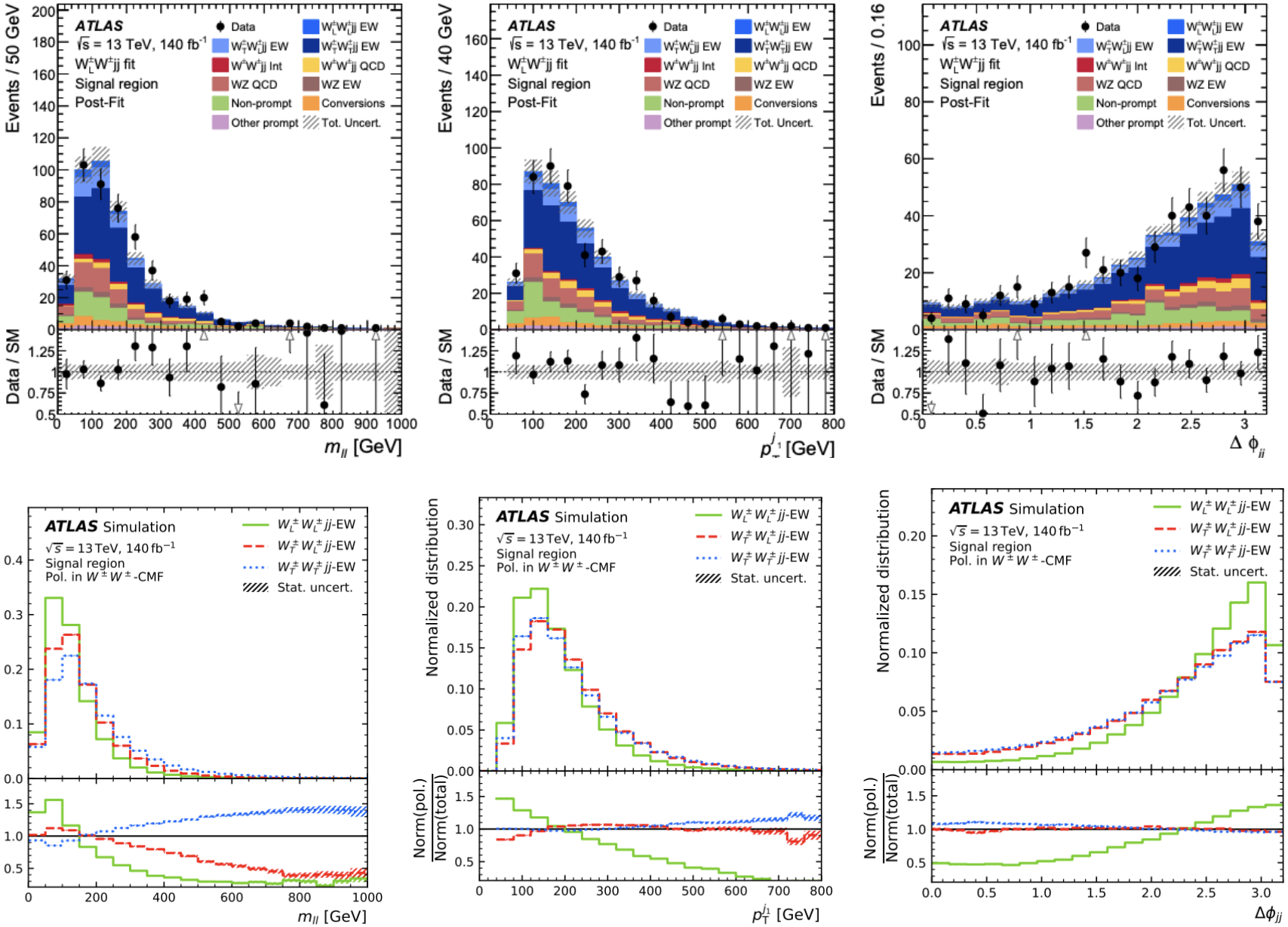

Longitudinally polarized W bosons in the electroweak production of same-sign W boson pairs in association with two jets (arXiv:2503.11317)

$W^{\pm}W^{\pm} \rightarrow \ell^{\pm}\nu\ell'^{\pm}\nu$ ➔ where ℓ and ℓ' can be e or μ

NEW March 2025!!!

Kinematics	Descriptions	Scaling
	Object-level variables	
$p_{\mathrm{T}}^{\ell_1}$	p_T of the leading lepton	$\log_{10}(x)$
η^{ℓ_1}	η of the leading lepton	x
ℓ_1 type	Flavor of the leading lepton	x
$p_{\mathrm{T}}^{\ell_2}$	p_{T} of the subleading lepton	$\log_{10}(x)$
η^{ℓ_2}	η of the subleading lepton	x
$\phi^{\ell_2} - \phi^{\ell_1}$	Difference in azimuthal angle between the leading and subleading leptons	x
ℓ_2 type	Flavor of the subleading lepton	x
$p_{\mathrm{T}}^{j_1}$	p_{T} of the leading jet	$\log_{10}(x)$
η^{j_1}	η of the leading jet	x
$\phi^{j_1} - \phi^{\ell_1}$	Difference in azimuthal angle between the leading jet and leading lepton	x
$p_{\mathrm{T}}^{j_2}$	p_{T} of the subleading jet	$\log_{10}(x)$
η^{j_2}	η of the subleading jet	x
$\phi^{j_2} - \phi^{\ell_1}$	Difference in azimuthal angle between the subleading jet and leading lepton	x
$E_{\mathrm{T}}^{\mathrm{miss}}$	Missing transverse momentum	$\log_{10}(x)$
$\phi(E_{\mathrm{T}}^{\mathrm{miss}}) - \phi^{\ell_1}$	Difference in azimuthal angle between the missing transverse momentum and leading lepton	x
	Event-level variables	
$Z_{\ell_1}^{\star}$	Zeppenfeld variable of the leading lepton [64]	$\sqrt{x}$
$Z_{\ell_2}^{\star}$	Zeppenfeld variable of the subleading lepton [64]	$\sqrt{x}$
$m_{\mathrm{T}}^{\ell_1}$	Transverse mass of the leading lepton and $E_{\mathrm{T}}^{\mathrm{miss}}$	$\sqrt{x}$
$m_{\mathrm{T}}^{\ell_2}$	Transverse mass of the subleading lepton and $E_{\mathrm{T}}^{\mathrm{miss}}$	$\sqrt{x}$
$\Delta R_{\ell\ell}$	Distance ΔR between the leading and subleading leptons	x
$\Delta\eta_{\ell\ell}$	Difference in pseudorapidity between the leading and subleading leptons	$\sqrt{x}$
$m_{\ell\ell}$	Invariant mass of the two leptons	$\log_{10}(x)$
$p_{\mathrm{T}}^{\ell\ell}$	p_{T} of the dilepton system	$\sqrt{x}$
m_{T}	Transverse mass of the dilepton system and $E_{\mathrm{T}}^{\mathrm{miss}}$ [20]	$\sqrt{x}$
m_{T}^{o}	Projected transverse mass $\sqrt{(p_{\mathrm{T}}^{\ell_1} + p_{\mathrm{T}}^{\ell_2} + E_{\mathrm{T}}^{\mathrm{miss}})^2 - (\vec{p_{\mathrm{T}}}^{\ell_1} + \vec{p_{\mathrm{T}}}^{\ell_2} + \vec{E}_{\mathrm{T}}^{\mathrm{miss}})^2}$ [65]	$\sqrt{x}$
ΔR_{jj}	Distance ΔR between the leading and subleading jets	x
Δy_{jj}	Rapidiy difference between the leading and subleading jets	x
m_{jj}	Invariant mass of the two jets	$\log_{10}(x)$
$\Delta\phi_{jj}$	Difference in azimuthal angle between the leading and subleading jets	x
$(p_{\mathrm{T}}^{\ell_1} \cdot p_{\mathrm{T}}^{\ell_2})/(p_{\mathrm{T}}^{j_1} \cdot p_{\mathrm{T}}^{j_2})$	p_{T} ratio of the leptons and jets [22]	$\log_{10}(x + 0.02)$
$\min(\Delta R_{\ell,j})$	Minimal distance ΔR between the leptons and jets	x

Variables used in the training and optimization of the DNNs. The variables are scaled with different scaling functions for the training and application.